Ultrafast Electron Transfer in the Complex between Fluorescein and a Cognate Engineered Lipocalin Protein, a So-Called Anticalin†

M. Götz,‡ S. Hess,‡ G. Beste,§,|| A. Skerra,*,§ and M. E. Michel-Beyerle*,‡

Institut für Physikalische und Theoretische Chemie, Technische Universität München, 85748 Garching, Germany, and Lehrstuhl für Biologische Chemie, Technische Universität München, 85350 Freising-Weihenstephan, Germany

Received October 25, 2001

ABSTRACT: Anticalins are a novel class of engineered ligand-binding proteins with tailored specificities derived from the lipocalin scaffold. The anticalin FluA complexes fluorescein as ligand with high affinity, and it effects almost complete quenching of its steady-state fluorescence. To study the underlying mechanism, we have applied femtosecond absorption spectroscopy, which revealed excited-state electron transfer within the FluA·Fl complex to be responsible for the strong fluorescence quenching. On the basis of a comparison of redox potentials, either tryptophan or tyrosine may serve as electron donor to the bound fluorescein group in its excited singlet state, thus forming the fluorescein trianion radical within 400 fs. The almost monoexponential rate points to a single, well-defined binding site, and its temperature independence suggests an (almost) activationless process. Applying conventional electron transfer theory to the ultrafast forward and slower back-rates, the resulting electronic interaction is rather large, with ∼140 cm^{-1} for tyrosine, which would be consistent with a coplanar arrangement of both aromatic moieties within van der Waals distance. The weak residual steady-state fluorescence originates from a small (∼10%) component with a time constant in the 40−60 ps range. These results demonstrate the power of time-resolved absorption spectroscopy as a diagnostic tool for the elucidation of a fluorescence quenching mechanism and the temporal profiles of the processes involved. The high structural and dynamic definition of the complexation site suggests the anticalin FluA to be a promising model in order to tailor and probe electronic interactions and energetics in proteins.

The bright green emission[1] of the fluorescein dianion, its easy synthesis, and its high chemical stability are responsible for its widespread application as a reporter pigment in chemistry and, in particular, in the biological sciences. Fluorescein and its chemically activated derivatives are generally used for the covalent labeling of biomacromolecules, including nucleic acids, proteins, and especially antibodies. Thus, many phenomena in biochemistry, cell biology, and even medicine can be studied by means of sensitive detection techniques, for example, via fluorescence microscopy, fluorescent cell sorting, and quantitative fluorometry. Due to the population of different prototropic forms (*4*) the free compound can also be used as a fluorescent pH indicator within cellular compartments.

Apart from that, fluorescein has been found to elicit a strong immune response when conjugated with a protein carrier and therefore extensively served as a hapten in immunological studies (*5*). The fluorescein-binding monoclonal antibody 4-4-20 was thoroughly characterized, including elucidation of its crystal structure at high resolution (*6*, *7*) and bacterial production and biochemical analysis as a single-chain Fv fragment (*8*). Antibodies raised against the fluorescein group often show a pronounced fluorescence quenching effect upon binding of this ligand. For example, in the case of the recombinant 4-4-20 single-chain Fv fragment $Q_{max} = 85.9 \pm 0.4\%$ was measured (*8*). Such antibodies with high affinity and quenching effect on fluorescein have also been utilized in special experimental applications, e.g., to determine the orientation of transmembrane proteins that were site-specifically labeled with fluorescein (*9*) or to discriminate between free and bound states of a fluorescein-conjugated peptide ligand in cell surface receptor-binding studies (*10*).

More recently, fluorescein was employed as a model target for the generation of a cognate anticalin, i.e., an engineered lipocalin protein (*11*). Lipocalins are small monomeric ligand-binding proteins, which naturally play a role in the transport or storage of lipophilic or chemically sensitive physiological compounds, for example, biliverdin IX_γ in the case of the bilin-binding protein (BBP). Proteins of the lipocalin family share a characteristic polypeptide fold

† M.E.M.-B. gratefully acknowledges financial support by the Deutsche Forschungsgemeinschaft (SFB 533) and the Volkswagenstiftung. A.S. thanks the Fonds der Chemischen Industrie for financial support.

* Corresponding authors. M.E.M.-B.: telephone, (+49) 89 289 13400; fax, (+49) 89 289 13026; e-mail, michel-beyerle@ch.tum.de. A.S.: telephone, (+49) 8161 71 4351; fax, (+49) 8161 71 4352; e-mail, skerra@wzw.tum.de.

‡ Institut für Physikalische und Theoretische Chemie, Technische Universität München.

§ Lehrstuhl für Biologische Chemie, Technische Universität München.

|| Present address: Xerion Pharmaceuticals, 82152 Martinsried, Germany.

[1] The fluorescence quantum yield of the fluorescein dianion was reported to be 0.93 (*1*−*3*).

10.1021/bi015888y CCC: $22.00
Published on Web 03/03/2002

comprising a circularly closed eight-stranded antiparallel β-sheet. This β-barrel is usually open to the solvent on one side and a set of four loops, each connecting a pair of neighboring β-strands, forms the entry to the ligand pocket. Contrasting with the structurally conserved β-barrel, the loops vary considerably in length and conformation among different lipocalins and thus determine their ligand specificities (*12*). Thus, the lipocalin architecture resembles that of immunoglobulins, where a set of six hypervariable loops that are supported on top of a rigid β-sheet framework makes up the antigen-binding site.

In an attempt to reshape the ligand pocket of the BBP via combinatorial protein design, the fluorescein group served as a target for molecular recognition (*11*). Using the methods of site-directed random mutagenesis and phage display (*13*) an engineered lipocalin, the anticalin FluA, was selected with high affinity for fluorescein (K_D = 35.2 ± 3.2 nM). Unexpectedly, and contrasting with other cognate anticalins that were selected along with FluA (*11*), this protein exerted an almost complete quenching effect on the steady-state ligand fluorescence upon complexation of fluorescein (Q_{max} = 99.7 ± 0.3%). This extraordinary phenomenon, which surpasses quenching effects described so far for anti-fluorescein antibodies, prompted an investigation of the underlying physicochemical mechanism.

Here, we describe time-resolved absorption measurements at the femtosecond scale that allow us to identify the excited molecular states and their temporal population. On the basis of our results, we propose a mechanism involving an initial ultrafast electron transfer between the protein and the bound fluorescein.

MATERIALS AND METHODS

Materials. FluA was prepared as a recombinant protein by secretion into the periplasm of *Escherichia coli* and purified by means of the *Strep* tag as described (*11*). Fluorescein was purchased as a sodium salt from Sigma Deisenhofen, Germany, and a stock solution was prepared by dissolving 36.4 mg of fluorescein in 100 mL of phosphate-buffered saline (PBS)/1 mM EDTA (pH = 8.0). The FluA·Fl samples used for all measurements contained 18 μL of fluorescein stock solution (967 μM) added to 150 μL of the FluA protein at 190 μM, dissolved in the same buffer.

Spectroscopic Methods. Steady-state absorption spectra were recorded with a UV−vis spectrometer (Perkin-Elmer Lambda 2S) at 2.0 nm resolution, and fluorescence spectra were measured using a spectrofluorometer (Spex Fluorolog-2 Model F212I) with 1.7 nm resolution or better.

Our methodology of time-resolved measurements was based on the sample's absorption when probed at specific wavelengths in the absence or presence of illumination (difference absorption). For these transient absorption measurements a Ti:sapphire oscillator/regenerative amplifier system, which has been described in detail elsewhere (*14*), was used. Briefly, the output at 780 nm of an Ar^+ laser-pumped commercial Ti:sapphire oscillator (MIRA/Coherent, repetition rate 76 MHz, pulse width 100 fs) was temporarily broadened to 150 ps before seeding a regenerative amplifier system (BMI Alpha 1000S) pumped at 10 W by a Nd:YLF laser (BMI 621D) at 528 nm. The amplified pulses (1.4 mJ) were split into a pump and a probe beam (9:1). After separate recompression optical pulses at 780 nm with a pulse duration of 120 fs were obtained. The pump pulses were frequency-doubled and directed through an optical parametric generator and amplifier setup to produce a signal wave at 495 nm for excitation. The weaker probing pulses passed a variable delay line (up to 5 ns) and were focused in a 2 mm sapphire crystal to produce a white light continuum. A chirp-compensated stepper motor-controlled spectrometer was used to select spectral regions with a bandwidth of 12 nm. The relative polarizations between pump and probe beam were set to the magic angle (54.7°) to avoid rotational depolarization effects. Pump and probe beams were focused under a mutual angle of 10° at a cuvette with 1 mm path length containing the sample.

The experimental data were fitted to a multiexponential decay function convoluted with the instrument response function $B(t - t_0)$ centered at t_0:

$$\Delta A(t) = \int_0^\infty \left(\Delta A_0 + \sum_{i=1}^{n} \Delta A_i \exp\left(-\frac{t'}{\tau_i} \right) \right) B(t - t' - t_0)\, dt' \quad (1)$$

Here $\Delta A(t)$ is the difference absorption at time t, ΔA_i is the amplitude of the component with lifetime τ_i, and ΔA_0 is the offset due to long-living species. The instrument response function was modeled by a Gaussian with a variable full width half-maximum (fwhm, typically 250 fs).

For better illustration of the short time kinetics, the measurements depicted in Figure 3 address a time window of less than 5 ps from which the ultrashort time components were derived. These were used as fixed parameters in the fitting procedures of data sets that extended into the nanosecond range.

RESULTS

Steady-State Spectroscopy of Free and Protein-Bound Fluorescein. Steady-state absorption, fluorescence, and fluorescence excitation spectra of free fluorescein and of fluorescein bound to the anticalin (FluA·Fl) are compared in Figure 1, both in aqueous buffer solution at pH 8.0. If not otherwise stated, fluorescence was excited at 490 nm, and fluorescence excitation was probed at 540 nm. The maxima of both spectra were normalized with respect to the absorption peak at 490 nm. In Figure 1a the shape and peak position of the intense absorption band at 490 nm are typical for fluorescein in its dianionic state, which is the predominant protolytic form at pH 8.0 (*4*, *15*). This absorption band corresponds to the $\pi-\pi^*$ transition of the xanthene ring; the shoulder at 460−475 nm has been attributed to the $1 \leftarrow 0$ transition of the totally symmetric ring breathing mode (*16*). In the FluA·Fl complex this shoulder develops into a pronounced peak at 460 nm, whereas the weak absorption band at shorter wavelengths around 323 nm seems to be independent of the complexation. The similarity of the two absorption spectra in Figure 1 suggests that fluorescein is bound to the protein in its dianionic state whereby the appearance of a pronounced vibronic band progression with a typical energy separation of about 1330 cm^{-1} reflects a reduction in the degrees of freedom, which is typical for a tight binding situation. In FluA·Fl the UV band at 283 nm of the ligand is superimposed by the intense absorption of

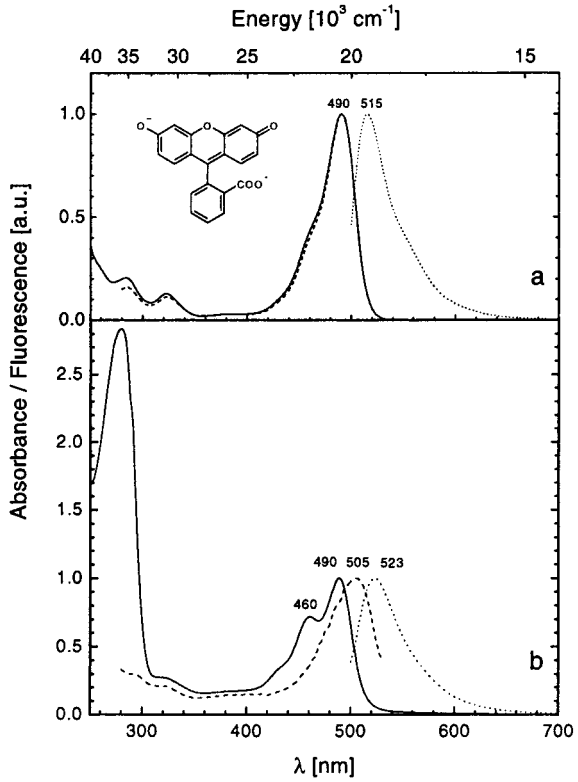

FIGURE 1: Normalized steady-state absorption (—), fluorescence (•••), and fluorescence excitation (- - -) spectra of (a) free fluorescein and (b) fluorescein bound to FluA (FluA·Fl) both in buffer, pH 8.0, at $T = 295$ K. Fluorescence was excited at 490 nm, and fluorescence excitation was probed at 540 nm.

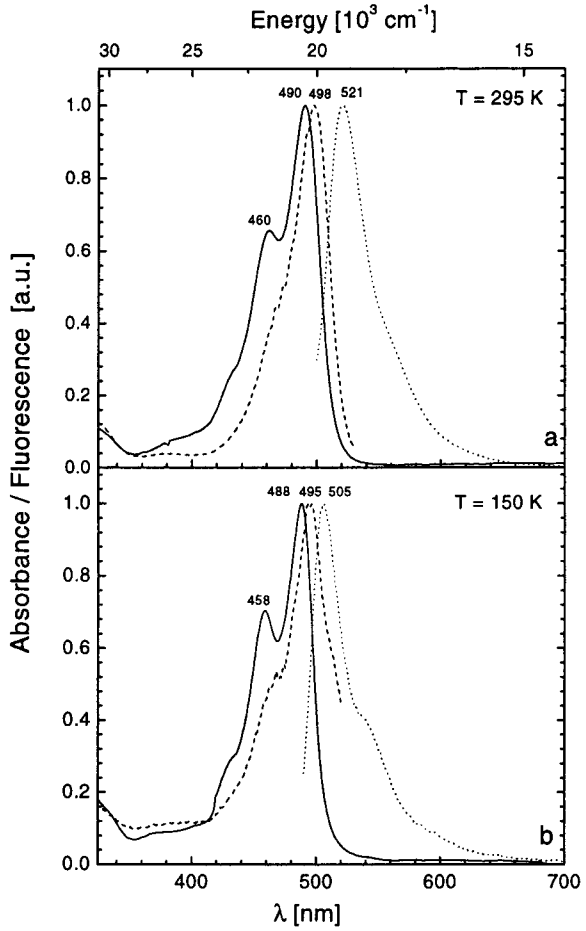

FIGURE 2: Normalized steady-state absorption (—), fluorescence (•••), and fluorescence excitation (- - -) spectra of FluA·Fl in 60% glycerol/buffer, pH 8.0, at 295 K (a) and 150 K (b). For 295 K fluorescence was excited at 490 nm whereas for 150 K it was excited at 480 nm. Excitation was probed at 540 nm for both temperatures.

the protein, predominantly caused by aromatic side chains of tryptophan (Trp) and tyrosine (Tyr).

Regardless of the excitation wavelength, the fluorescence spectrum of FluA·Fl is red shifted as compared to the free chromophore in solution (Figure 1a). In addition, the fluorescence excitation spectrum of FluA·Fl does not follow its absorption spectrum. It is red shifted by 15 nm, and the vibronic shoulder at 460 nm is missing, together with the protein peak at 280 nm. This dramatic red shift implies that the fluorescence of the majority population of the bound fluorescein is quenched and only a small subpopulation is responsible for the fluorescence. The fluorescence excitation spectrum with its peak at 505 nm is characteristic for the absorption spectrum of this subpopulation. The intensity of this minority emission is within the previously published fraction of ~0.3% (*11*). Moreover, this subpopulation of bound fluorescein cannot be excited in the protein absorption band at 280 nm, as shown in Figure 1b. This points to suppression of energy transfer from aromatic amino acids due to a larger distance and/or an unfavorable geometry. Nevertheless, this minority population is characterized by a Stokes shift of 680 cm^{-1} (Figure 1b), which reflects its complexation by the protein since it is about 310 cm^{-1} smaller than the one measured for the free chromophore.

To gain insight into the fluorescence quenching mechanism, steady-state and time-resolved measurements at low temperatures are useful, even though they require the presence of a cryoprotector. The experimental conditions of a glassy matrix necessary for low-temperature absorption studies were met with an aqueous protein solution containing 60% glycerol. As shown in Figure 2a the effect of glycerol on the absorption and fluorescence spectra of FluA·Fl at room temperature is negligible. This is not the case for the excitation spectrum, which is blue shifted by 6−7 nm. If we again attribute the fluorescence excitation spectrum to the absorption of a less quenched minority population, it is obvious that addition of glycerol leads to an increase of the fluorescing minority population. This effect is consistent with a pronounced gain in the overall fluorescence intensity that was observed in these steady-state measurements.

An analogous set of spectra was recorded at low temperatures ranging from 295 to 90 K. The spectra in Figure 2b taken at 150 K are representative for low temperatures since further cooling was of no effect. At low temperatures the shoulder in the red wing of the fluorescence spectrum gains intensity, together with the appearance of a more pronounced vibronic structure and narrowing of the absorption bands. The peak position of the absorption band remains grossly unchanged whereas the maximum of the fluorescence band shifts by 15 nm to the blue. In contrast to room temperature (Figure 2a), where the excitation spectra were invariant when probed in the maximum or in the red wing of the fluorescence band, this was not the case at low temperatures (not shown). For example, the peak position of the fluorescence excitation spectrum shifted from 495 to 501 nm when probed at 540 or 560 nm, respectively. This behavior reflects the combined

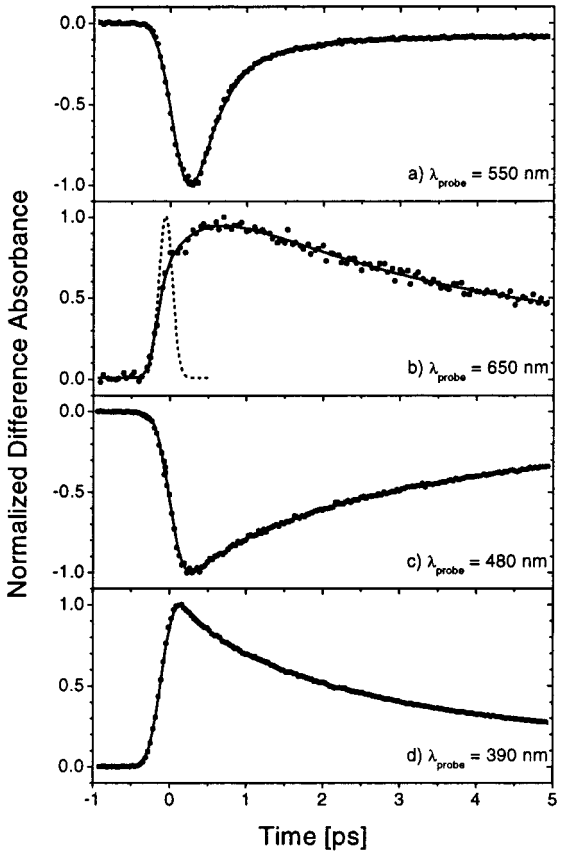

FIGURE 3: Dependence of temporal evolution of difference absorbance of FluA·Fl following excitation at 495 nm, probing (a) stimulated emission from $^1(Fl^{2-})^*$ at 550 nm and (b) the formation of a product state at 650 nm. To clearly demonstrate the rise characteristics, the instrument response function (fwhm = 250 fs) is included (···). (c) The recovery of the Fl^{2-} ground state absorption was probed at 480 nm, and (d) the superimposed absorption of both the excited state $^1(Fl^{2-})^*$ and either the radical trianion $(Fl^{3-})^\bullet$ or the radical monoanion $(Fl^{1-})^\bullet$ was measured at 390 nm. The solid lines are best fits, which led to the time components and amplitudes listed in Table 1.

effects of glycerol and cooling, which lead to an increased spectral dispersion. This effect is due to some loss of structural definition of the fluorescein binding site, which lowers the probability of fluorescence quenching.

In summary, the feature of a red-shifted fluorescence excitation spectrum of the FluA·Fl complex is characteristic for the absorption of a fluorescing minority population. Addition of the cryoprotector glycerol leads to an increase of this minority emission concomitant with a slight blue shift of the excitation spectrum. At low temperatures the fluorescence excitation spectrum tends to depend also on the probing wavelength. This feature is equivalent to the notion that, upon lowering the temperature, the absorption spectrum of the fluorescing minority becomes increasingly dispersive, reflecting multiple binding sites with decreased quenching efficiency.

Femtosecond Transient Absorption Spectroscopy of the FluA·Fl Complex. The protein−fluorescein complex was excited in its absorption peak at 495 nm, and the temporal evolution of the following species was monitored in specific spectral regions:

(a) *The initially excited state* $^1(Fl^{2-})^*$ was probed in the stimulated emission region at 550 nm (Figure 3a). This

Table 1: Numerical Parameters of the Fit Functions Displayed in Figure 3 for the Different Spectral Regions of Probing (λ_{probe})[a]

λ_{probe} (nm)	ΔA_1 (%)	τ_1 (ps)	ΔA_2 (%)	τ_2 (ps)	ΔA_3 (%)	τ_3 (ps)
550	−93	0.42			−7	60
650	−57	0.45	76	3.1	24	37
480	−24	0.52	−67	4.0	−9	42
390	28	0.43	61	3.4	11	49

[a] $\Delta A_{1,2,3}$ denote the relative amplitudes belonging to the time constants $\tau_{1,2,3}$. The short time constants τ_1 have been determined within the time window of 5 ps as depicted in the figure, using small increments between the reading points. The longer time constants τ_2 and τ_3 have been fitted using the full time window of 5 ns (not shown).

wavelength in the red wing of the fluorescence band has been chosen in order to minimize contributions of ground state absorption. Under these conditions the negative difference absorption mirrors an apparently increased transmission due to a photon-stimulated depletion of the excited state. Thus, the stimulated emission measured in absorption reports on the excited-state lifetime in a fashion similar to that of a time-resolved fluorescence measurement.

(b) *A potential product of the quenching process* was probed at 650 nm in a spectral region where both its formation and decay kinetics can be resolved (Figure 3b).

(c) *The recovery of the ground state absorption of* (Fl^{2-}) was probed at 480 nm (Figure 3c), i.e., in the blue wing of the main absorption band (Figure 1) in order to eliminate contribution from stimulated emission.

(d) *The product state* was also investigated at 390 nm (Figure 3d). At this wavelength the two one-electron redox states of the fluorescein dianion, the oxidized $(Fl^{1-})^\bullet$ and the reduced $(Fl^{3-})^\bullet$ species, absorb with comparable extinction coefficients (*17*, *18*).

At all probing wavelengths the contribution of the fluorescing minority appeared to be negligible since the kinetics did not depend on the excitation wavelength in the blue wing of the absorption band (475 or 455 nm), where the contribution of the minority should vary drastically according to its excitation spectrum depicted in Figure 1b.

(a) FluA·Fl in Aqueous Buffer at 295 K. Lifetime of $^1(Fl^{2-})^*$ *Probed at 550 nm.* The negative difference absorption shown in Figure 3a is the stimulated emission, which decays with time constants of $\tau_1 = 420$ fs and $\tau_2 = 60$ ps (Table 1). The large amplitude of 93% for the femtosecond component implies almost monoexponential kinetics. The time constant for the decay of the singlet excited fluorescein dianion in the protein pocket is by 4 orders of magnitude faster than the known decay time of 4.1 ns of the dianion in aqueous solution (*15*). This defines a fluorescence quantum yield of $\sim 10^{-4}$, which is in agreement with the previous fluorescence quenching value of 99.7 ± 0.3% from comparative steady-state measurements (*11*).

The central question arising from this observation of an ultra-short-lived excited state pertains to the mechanism of the quenching process and, in particular, to the notion whether the ultrafast decay of $^1(Fl^{2-})^*$ leads to the formation of a defined product. Such a product should arise with the decay kinetics of the precursor, i.e., the excited state.

(b) Formation and Decay of a Product State Probed at 650 nm. At this wavelength a rise component (indicated by the negative sign of the amplitude in Table 1) evolves with a time constant of $\tau_1 = 450$ fs (Figure 3b), which is similar

Scheme 1: Kinetic Scheme for the Mechanism of Fluorescence Quenching in FluA·Fl[a]

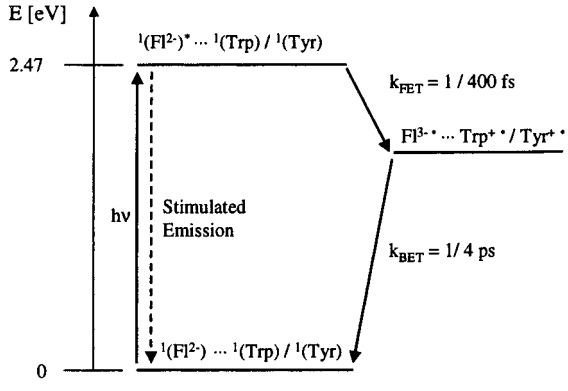

[a] Experimental conditions did not allow to discriminate between the potential electron donors Trp and Tyr.

to the one observed for the stimulated emission at 550 nm (Figure 3a). This feature indicates the formation of a product state. Its subsequent decay can be fitted with two exponentials, having a predominant time constant of $\tau_2 = 3.1$ ps and, in resemblance with the stimulated emission region, a small component with a time constant $\tau_3 = 37$ ps. The apparent question whether the decay of this product state leads to the recovery of ground state absorption again can be tested by tuning the wavelength of the probe beam to the corresponding spectral region.

(c) Recovery of (Fl^{2-}) Ground State Absorption Probed at 480 nm. At this wavelength a negative absorbance is observed due to bleaching of the ground state, which recovers in a multiexponential fashion (Figure 3c). In fact, the dominant component, with $\tau_2 = 4.0$ ps (67%), resembles the decay of the product state observed above. Therefore, already at this stage a three-level reaction cycle may be postulated (Scheme 1). The ultrafast component in this recovery pattern with a time constant $\tau_1 = 520$ fs (24%) is similar to the one observed when probing either the stimulated emission at 550 nm (Figure 3a) or the formation kinetics of the product state at 650 nm (Figure 3b). Therefore, it reflects the increase of absorption due to product formation. Similarly to the time traces monitored at 550 and 650 nm the recovery pattern is contaminated with a small slower component $\tau_3 = 42$ ps.

With respect to the quenching mechanism the sequence of processes depicted in Scheme 1 excludes a variety of processes, e.g., ultrafast internal conversion, irreversible photochemical bond splitting, and, considering the femtosecond time scale, also intersystem crossing. Furthermore, excited-state proton transfer appears to be improbable since the fluorescein dianion $^1(Fl^{2-})^*$ does not carry a proton with increased acidity. Hence, we claim that the excited-state reaction cycle is initiated by an ultrafast electron transfer, involving either oxidation or reduction of the fluorescein dianion. Since the absorption bands of both possible products at 390 nm are superimposed with comparable extinction coefficients (*17*, *18*), the redox process per se can be followed, even though its direction cannot be determined.

(d) Decay of Product State, (Fl^{1-})$^\bullet$ or (Fl^{3-})$^\bullet$, Probed at 390 nm. When the absorbance is monitored at 390 nm, an instant rise followed by three decay components is observed (Figure 3d): $\tau_1 = 430$ fs (28%), $\tau_2 = 3.4$ ps (61%), and

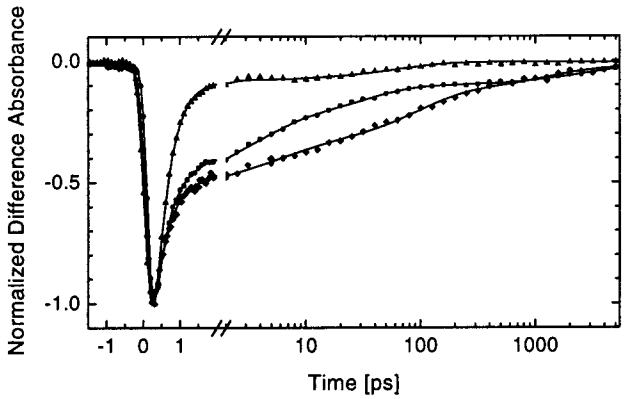

FIGURE 4: The decay of stimulated emission from FluA·Fl in (▲) aqueous buffer, pH 8.0, at $T = 295$ K, (●) 60% glycerol/buffer, pH 8.0, at $T = 295$ K, and (◆) 60% glycerol/buffer, pH 8.0, frozen matrix at $T = 150$ K. The excitation and probing wavelengths were 495 and 550 nm, respectively. Solid lines represent best fits; the resulting amplitudes and time components are compiled in Table 2.

Table 2: Numerical Parameters of the Fit Functions Displayed in Figure 4[a]

T (K)	ΔA_1 (%)	τ_1 (ps)	ΔA_2 (%)	τ_2 (ps)	ΔA_3 (%)	τ_3 (ps)	ΔA_4 (%)	τ_4 (ps)
295[b]	−93	0.42			−7	60		
295[c]	−66	0.35	−17	3.3	−17	32	−11	2900
150[c]	−65	0.37	−11	5.0	−16	87	−8	1300

[a] $\Delta A_{1,2,3,4}$ denote the relative amplitudes belonging to the time constants $\tau_{1,2,3,4}$. [b] FluA·Fl in aqueous buffer, pH 8.0. [c] FluA·Fl in 60% glycerol/buffer mixture, pH 8.0.

$\tau_3 = 49$ ps (11%). At this probe wavelength the absorption of $(Fl^{1-})^\bullet$ and $(Fl^{3-})^\bullet$ and of the fluorescein excited state $^1(Fl^{2-})^*$ is superimposed (*17*, *18*). Unfortunately, the relative extinction coefficients of all these species seem to be similar but are not very reliable. This uncertainty is particularly related to difficulties in the measurement of the extinction coefficient ϵ_{390} of $^1(Fl^{2-})^*$ (*17*). However, the fact that, upon probing at 390 nm, a ~400 fs rise component corresponding to the formation kinetics of the product state is not observed is indicative of the extinction coefficient ϵ_{390} of $^1(Fl^{2-})^*$ being larger by about a factor of at least 2 than ϵ_{390} of $(Fl^{3-})^\bullet$ or ϵ_{390} of $(Fl^{1-})^\bullet$, thus masking the rise dynamics.

FluA·Fl in a Buffer/Glycerol Glass Matrix at 295 K and at Low Temperatures. Lifetime of $^1(Fl^{2-})^*$ Probed at 550 nm. Figure 4 compares stimulated emission signals of FluA·Fl under different conditions: in aqueous buffer (i) as well as in a 60% glycerol/buffer mixture at 295 K (ii) and at 150 K (iii). In the presence of glycerol the decay of the excited state at high and low temperature is multiexponential and can be fitted with at least three time components, the shortest being $\tau = 420$ fs (93%) at 295 K and $\tau = 370$ fs (65%) at 150 K. Thus, the value of the shortest component is almost identical in all three cases, indicating a temperature-independent quenching process for the majority population of FluA·Fl.

DISCUSSION

Mechanism of Fluorescence Quenching in FluA·Fl. The key features of the quenching kinetics of the protein-bound fluorescein are its excited-state electron transfer within 400 fs, forming an intermediate radical ion pair, which recom-

bines within 4 ps (Scheme 1). Notably, the excited-state lifetime, and thus the primary electron transfer rate, is monoexponential, which points to a highly defined binding site.

The most probable partner for the excited fluorescein dianion to undergo electron transfer is a nearby aromatic amino acid with an appropriate redox potential. Trp and Tyr residues are suitable candidates since their own fluorescence has been shown to be quenched upon excitation at 280 nm when titrating FluA with variable amounts of fluorescein (*11*). The potency of Trp and Tyr as quenchers of excited fluorescein has also been discussed in the context of other spectroscopic assays: (i) screening of individual L-amino acids for the ability to quench fluorescein fluorescence in neutral aqueous solution resulted in the finding that L-Trp and, to a lesser degree, L-Tyr are effective quenchers (9); (ii) steady-state fluorescence quenching has also been observed in anti-fluorescein monoclonal antibodies such as 4-4-20 (*8*), whose combining sites are rich in Trp and Tyr residues and which are functionally related to the FluA·Fl complex. FluA contains 15 Tyr and 6 Trp residues (plus a further Trp as part of the *Strep* tag). Several of the Trp side chains are located close to the bound fluorescein within the β-barrel structure.

The feasibility and direction of excited-state electron transfer with respect to the change in free energy can be tested using the Rehm−Weller expression (*19*):

$$\Delta G_{FET} = E^{ox}(D/D^{+\bullet}) - E^{red}(A/A^{-\bullet}) - \Delta E_{00} - e^2/4\pi\epsilon_0\epsilon R \quad (2)$$

where $E^{ox}(D/D^{+\bullet})$ and $E^{red}(A/A^{-\bullet})$ refer to the oxidation potential of the electron donor and the reduction potential of the electron acceptor, respectively. ΔE_{00} is the electronic excitation energy corresponding to the energy gap between the vibronic ground and first excited singlet states ($S_{0,0} \rightarrow S_{1,0}$); ϵ is the static dielectric constant, ϵ_0 the permittivity of the vacuum, and R the distance between donor and acceptor. The Coulombic term is difficult to estimate as the donor−acceptor distance and orientation as well as the local dielectric constant are unknown. Since this term can only increase the driving force, it is neglected in the following estimates on the directionality of the forward electron transfer.

The redox potentials are taken from electrochemical data. At pH = 7.0 the oxidation potential of Tyr in aqueous solution $E^0[Tyr^{+\bullet}/Tyr] = 0.66$ V (SCE) (*20*). It becomes less positive at increasing pH, thereby facilitating forward electron transfer (FET); e.g., $E^0[Tyr^{+\bullet}/Tyr] = 0.58$ V (SCE) at pH = 8.0. The analogous oxidation potentials for Trp at neutral pH and pH = 8.0 are $E^0[Trp^{+\bullet}/Trp] = 0.75$ V (SCE) and $E^0[Trp^{+\bullet}/Trp] = 0.69$ V (SCE), respectively (*20*). The reduction potential of the fluorescein dianion, which is stable with a pK_a of 6.3, is $E^0[Fl^{2-}/Fl^{3-\bullet}] = -1.19$ V (SCE) (*21*), and its ($S_{0,0} \rightarrow S_{1,0}$) excitation energy is 2.47 eV.

With the assumptions that, within the binding pocket the difference in redox potentials is maintained and the contribution of the Coulombic interaction to the driving force is neglected, the driving force for the forward electron transfer involving Trp and Tyr is $\Delta G_{FET} = -0.59$ eV and $\Delta G_{FET} = -0.7$ eV, respectively. These ΔG values clearly indicate the energetically favorable direction of photoinduced electron transfer either from Trp or from Tyr to the fluorescein dianion. Notably, the excited-state lifetime, and thus the primary electron transfer rate, is monoexponential, which points to a highly defined binding site. However, because the Coulombic interaction was omitted, these values can be only lower limits for forward electron transfer involving Trp or Tyr. Accordingly, upper limits for the back electron transfer (BET) repopulating the ground states of the fluorescein dianion and the neutral Trp and Tyr residues may be deduced as $\Delta G_{BET} \leq -1.88$ eV and $\Delta G_{BET} \leq -1.77$ eV for Trp and Tyr as the respective electron donors. More realistic energetics might be achieved by assuming a binding pocket which is weakly hydrophobic (see Appendix). Unfortunately, it is difficult to provide spectroscopic evidence for Trp and Tyr radical cations as likely product states since their absorption in the 500−550 nm region (*22*) coincides with the ground state bleaching of the fluorescein dianion as well as its stimulated emission.

Although a sufficiently negative driving force for photoinduced electron transfer to the fluorescein's excited state seems to exist, its probability is determined by the relation between driving force and reorganization energy for given electronic couplings as expressed in conventional electron transfer theory (see Appendix). Nevertheless, the observed ultrafast rate constant of forward electron transfer points (i) to close spatial proximity of donor and acceptor groups and (ii) to a (nearly) activationless process. From the experimental point of view the latter conclusion is confirmed by the temperature independence of the ultrafast component as illustrated in Figure 4.

In contrast to the forward electron transfer, the large driving force associated with the back electron transfer implies that k_{BET} is deeply buried in the Marcus inverted region (*23*) ($-\Delta G \gg \lambda_s$) and therefore slower (roughly by a factor of 10) as compared to k_{FET}. On the basis of electron transfer theory this rate should be weakly activated, and indeed, at low temperatures the average of slow components with lifetimes of ~4 ps at 295 K extends into the 20 ps range, which is consistent with this expectation.

Characterization of the Fluorescing Minority. As shown in Table 1, a 40−60 ps component appears in all spectral regions, indicating that such long components are common to both forward and back electron transfer processes. This observation implies that in a minority population the forward electron transfer is slowed by a factor of 100, in contrast to the reverse process, which is only by a factor of 10 slower than the respective process in the majority population. On the basis of theoretical arguments this result can be attributed to an increase of thermal activation energy of the forward rate that hardly affects the back electron transfer (see Appendix). Such effects might be caused by electrostatic interactions between the chromophore and its environment, e.g., by charged amino acid side chains near the binding cleft, which may adopt different conformations or protonation states. Such interactions may lead to a decrease in the driving force, creating a situation in the normal Marcus region ($-\Delta G < \lambda_s$). The easiest explanation would be a decrease of an already small Coulombic barrier by additional electrostatic screening (see Appendix).

Although the contribution of the 40−60 ps component to the overall kinetics is small with a relative amplitude of ~10%, it should be emphasized that it is this minority, with

its longer lifetime, that is mainly responsible for the low yield steady-state fluorescence shown in Figure 1. Despite the large amplitude (93%) of the 400 fs component of the stimulated emission its contribution to the steady-state fluorescence is at least 1 order of magnitude less than that of the 40−60 ps component. The spectral fingerprints of this fluorescing minority in FluA·Fl are the red-shifted fluorescence excitation spectrum (and correspondingly its characteristic absorption spectrum) and the relatively small Stokes shift of 680 cm^{-1}.

Similar features have been reported for fluorescein bound to antibodies, e.g., to the monoclonal anti-fluorescein antibody 4-4-20 (*24*, *25*). However, in contrast to FluA·Fl, measurements on different antibody systems revealed a pronounced red shift of the whole fluorescein absorption band ranging from 498 to 520 nm (*5*, *25*−*28*). This red shift in absorption has earlier been postulated as the fingerprint of antibody-bound fluorescein. Our findings with FluA·Fl do not support this conclusion as a general rule since the long-wavelength maxima of the absorption spectra in Figure 1 coincide. Instead, a comparison of both protein−ligand systems indicates that a red-shifted absorption spectrum correlates neither with the fluorescence quenching efficiency nor with the thermodynamic affinity for the fluorescein dianion.

CONCLUSIONS

(1) Femtosecond absorption spectroscopy applied to FluA·Fl revealed excited-state electron transfer to be responsible for the strong fluorescence quenching effect. On the basis of redox potentials either a tryptophan or tyrosine residue may serve as electron donor to the bound fluorescein in its excited singlet state, thus leading to the formation of the fluorescein trianion radical on the 400 fs time scale. This short time represents one of the fastest electron transfer reactions so far resolved in a protein at physiological temperature. In fact, this electron transfer time is by a factor 3−4 faster than the fastest step in photosynthesis at ambient temperature (*29*). For comparison, in the bacterial reaction center of *Rhodobacter sphaeroides* electron transfer from reduced bacteriochlorophyll to bacteriopheophytin proceeds with a time constant of ∼1−2 ps (*30*).

(2) Because excited-state quenching via electron transfer depends in a most sensitive way on the electronic interaction between the electron donor and acceptor, these processes are easily affected by structural changes involving the donor/acceptor species and their environment. Thus, unless complex compensation effects among the different parameters in electron transfer theory play a role (see Appendix), the almost monoexponential ultrafast decay kinetics of the excited fluorescein dianion that is observed for FluA·Fl points to a single, well-defined binding site. The electron donor tryptophan or tyrosine is likely to be located coplanar and in close proximity, as concluded from a comparison with an artificial cyclophane-bridged donor/acceptor system (see Appendix). Structural perturbations induced by external conditions, e.g., by the cryoprotector glycerol, were shown to induce dispersive slower kinetics as observed previously for a variety of other proteins (*31*, *32*).

(3) On the basis of conventional electron transfer theory globally applied to both the fast, activationless forward and slower back electron transfer rates, the electronic interaction involved in the electron transfer process is estimated to be ∼170 cm^{-1} (∼140 cm^{-1}) in the case of Trp (Tyr) assuming a polar environment, i.e., electrostatic screening of the Coulombic interaction. In the case of a more realistic weakly hydrophobic environment allowing still for local electrostatic interactions, the driving force would be increased by 0.2 eV and the electronic couplings would be decreased by about 20% if a static dielectric constant $\epsilon = 20$ and a center to center coplanar distance between the fluorescein dianion and the aromatic amino acid residue of 3.5 Å were assumed.

(4) The weak steady-state fluorescence is due to a 10% minority of FluA·Fl, which is characterized by its red-shifted absorption spectrum as reflected in the fluorescence excitation spectrum and by its excited-state lifetime of 40−60 ps.

(5) In principle, steady-state absorption and fluorescence excitation spectra as well as fluorescence quantum yields cannot provide information about the distribution of rates and thus do not distinguish between heterogeneous binding sites on one hand and distinct binding sites with reduced quenching efficiency on the other. In view of the strong interest in the structural characterization of hapten/antibody systems, in particular with respect to site-directed amino acid exchange, the experiments described in this paper underline the value of time-resolved spectroscopy as a unique diagnostic tool.

ACKNOWLEDGMENT

A.S. thanks S. Danzer for technical assistance.

APPENDIX

To perform a semiquantitative data analysis, forward and back electron transfer rates, k_{FET} and k_{BET}, are treated within the framework of electron transfer theory (*23*) using the nonadiabatic quantum mechanical approach (*33*−*35*). This theory gives the electron transfer rate k as the product of an electronic coupling matrix element (V) and a Franck−Condon weighted density of states FCWD:

$$k = \frac{4\pi^2}{h} V^2 \mathrm{FCWD} \tag{3a}$$

$$\mathrm{FCWD} = \sqrt{\frac{1}{4\pi\lambda_s k_B T}} \sum_{n=0}^{\infty} \frac{e^{-S} S^n}{n!} \exp\left(-\frac{(\Delta G + \lambda_s + n\hbar\omega)^2}{4\lambda_s k_B T}\right) \tag{3b}$$

$$S = \frac{\lambda_i}{\hbar\omega} \tag{3c}$$

The Franck−Condon term (eq 3b) includes the driving force (ΔG), which for photoinduced electron transfer is usually estimated on the basis of electrochemical redox potentials, excitation energy, and Coulombic interaction in case the product states are oppositely charged (eq 2). The low-frequency solvent and high-frequency intramolecular reorganization energies, λ_s and λ_i, are associated with the response of the respective modes to the change in charge distribution. Relevant for λ_s are the polar modes of solvent and protein while λ_i relates to a single averaged, high-

frequency molecular mode ω, which couples to the electron transfer process. This mode is often approximated by 1500 cm^{-1}, i.e., by a frequency corresponding to a typical skeletal vibration in an aromatic compound (*34*, *35*).

For a (nearly) barrierless forward electron transfer, as concluded from the ultrafast rate of 1/(400 fs), λ_s can be assumed to be approximately equal to $-\Delta G_{FET}$ or slightly smaller. The activationless nature of this rate is further corroborated by temperature-dependent measurements (Figure 4) where the ultrafast kinetic component is shown to be temperature independent. Assuming that neither energetic nor structural parameters are grossly affected by cooling, this result is consistent with both an activationless (or a weakly inverted) k_{FET} rate (*33*). The temperature independence of the 400 fs component also shows that the nonadiabatic approach (eq 3) is a good approximation for the treatment of these kinetic data. The insensitivity of the forward electron transfer rate to changes in temperature measured between 295 and 150 K indicates that the dynamics of the medium hardly influences the kinetics. In contrast, precisely such an effect would be expected for an adiabatic electron transfer process to which eq 3 would not apply.

Using eq 3 for an estimate of the parameters λ_i and V and basing this estimate on (i) the room temperature forward and backward rates, $k_{FET} = 1/(400\ fs)$ and $k_{BET} = 1/(4\ ps)$, (ii) activationless electron transfer, and (iii) a negligible contribution of the Coulombic term in eq 2, the resulting electronic couplings V and molecular reorganization energies λ_i are $V = 170\ (140)\ cm^{-1}$ and $\lambda_i = 0.42\ (0.32)$ eV for Trp (Tyr).

If we adopt a more realistic, slightly polar binding pocket and model such a situation globally by a static dielectric constant of $\epsilon = 20$, the contribution of the Coulombic term (eq 2) would amount to 0.2 eV for a coplanar center-to-center distance of 3.5 Å between Trp (Tyr) and the xanthene ring. Such a change in driving force would imply a decrease of both the electronic couplings V of $\sim 50\ cm^{-1}$ ($\sim 35\ cm^{-1}$) and the intramolecular reorganization energy λ_i of ~ 0.22 eV (~ 0.1 eV) for Trp (Tyr). Qualitatively, the binding pocket might be best characterized by strong $\pi-\pi$ interactions between the xanthene ring and a nearby Trp (Tyr) residue on one hand and by local electrostatic interactions between the negatively charged xanthene ring and charged or dipolar species on the other (e.g., local water molecules, charged or dipolar amino acid residues such as histidine, lysine, or arginine).

The crude parameter set proposed for activationless electron transfer in the FluA·Fl system comprising $-\Delta G \approx 0.6-0.8$ eV, $\lambda_i \approx 0.2-0.4$ eV, and $V \approx 120-170\ cm^{-1}$ seems to be quite reasonable. Some analogy might even exist between FluA·Fl and cyclophane-bridged porphyrin−quinone systems in solution (*36*). In the latter systems, where donor and acceptor are coplanar and in van der Waals contact, similar electron transfer rates in the range of $5 \times 10^{12}\ s^{-1}$ were observed. These rates were independent of the polarity of the solution and fitted within the framework of eq 3 to $\lambda_i \approx 0.54$ eV and $V \approx 140\ cm^{-1}$. Electronic interactions of this magnitude may be indicative of the proper juxtaposition of the aromatic amino acid side chain and the xanthene ring in FluA·Fl.

Qualitatively, electron transfer theory also allows to rationalize the slow kinetic components (40−60 ps) which occur with low amplitude and characterize the minority population responsible for the steady-state fluorescence. As these components are observed independent of the probing wavelength, it is concluded that for this minority population forward and back electron transfer rates have to be similar. One of the results of the quantum mechanical approach to electron transfer is the notion that small energy differences hardly affect an exoergic ($-\Delta G \gg \lambda_s$) electron transfer rate as k_{BET} which is expected to decrease only slightly with decreasing driving force. Thus, the pronounced slowing of τ_{BET} from 4 to $\sim$40 ps is mainly attributed to a decrease of the electronic coupling term V^2 due to a less defined binding site. Assuming an equal change in V^2 for the forward time constant τ_{FET}, the dramatic increase of the latter from 400 fs (observed for the majority) to $\sim$40 ps (observed for the fluorescing minority) would then be caused by almost equal contributions of a decrease in V^2 and an increase in the activation energy reflecting either an increase in λ_s or a decrease of ΔG_{FET}, or both. The assumptions of a weakly hydrophobic binding pocket for the majority and a more polar binding site for the minority would, in fact, explain a more activated forward rate of the minority where fluorescein is bound closer to the protein surface. For this minority the Coulombic interaction might indeed be negligible, thus reducing the driving force and shifting it into the normal Marcus regime ($-\Delta G < \lambda_s$).

REFERENCES

1. Weber, G., and Teale, F. W. J. (1957) *Trans. Faraday Soc. 53*, 646−655.
2. Hercules, D. M., and Frankel, H. (1960) *Science 131*, 1611−1612.
3. Seybold, P. G., Gouterman, M., and Callei, J. (1969) *Photochem. Photobiol. 9*, 229−242.
4. Klonis, N., and Sawyer, W. H. (1996) *J. Fluoresc. 6*, 147−157.
5. Voss, E. W. J. (1984) *Fluorescein Hapten: An immunological probe*, CRC Press, Boca Raton, FL.
6. Herron, J. N., Terry, A. H., Johnston, S., He, X.-M., Guddat, L. W., Voss, E. W. J., and Edmundson, A. B. (1994) *Biophys. J. 67*, 2167−2183.
7. Whitlow, M., Howard, A. J., Wood, J. F., Voss, E. W. J., and Hardman, K. D. (1995) *Protein Eng. 8*, 749−761.
8. Denzin, L. K., Gulliver, G. A., and Voss, E. W. J. (1993) *Mol. Immunol. 30*, 1331−1345.
9. Bar-Noy, S., Darmon, A., Ginsberg, H., and Cabantchik, Z. I. (1984) *Biochim. Biophys. Acta 778*, 612−614.
10. Sklar, L. A., Finney, D. A., Oades, Z. G., Jesaitis, A. J., Painter, R. G., and Cochrane, C. G. (1984) *J. Biol. Chem. 259*, 56661−56669.
11. Beste, G., Schmidt, F. S., Stibora, T., and Skerra, A. (1999) *Proc. Natl. Acad. Sci. U.S.A. 96*, 1898−1903.
12. Skerra, A. (2000) *Biochim. Biophys. Acta 1482*, 337−350.
13. Skerra, A. (2001) *Rev. Mol. Biotechnol. 74*, 257−275.
14. Pöllinger, F., Musewald, C., Heitele, H., Michel-Beyerle, M. E., Anders, C., Futscher, M., Voit, G., and Staab, H. (1996) *Ber. Bunsen-Ges. Phys. Chem. 100*, 2076.
15. Sjöback, R., Nygren, J., and Kubista, M. (1995) *Spectrochim. Acta A 51*, L7−L21.
16. Fleming, G. R., Knight, A. W. E., Morris, J. M., Morrison, R. J. S., and Robinson, G. W. (1977) *J. Am. Chem. Soc. 99*, 4306−4311.
17. Lougnot, D.-J., and Goldschmidt, C. R. (1980) *J. Photochem. 12*, 215−224.
18. Krüger, U., and Memming, R. (1974) *Ber. Bunsen-Ges. Phys. Chem. 78*, 670−678.
19. Weller, A. (1982) *Z. Phys. Chem. NF 133*, 93−98.

20. Harriman, A. (1987) *J. Phys. Chem. 91*, 6102−6104.
21. Coles, B. A., and Compton, R. G. (1983) *J. Electroanal. Chem. 144*, 87−98.
22. Pan, J., Lin, W., Wang, W., Zhan, Z., Lu, C., Yao, S., Lin, N., and Zhu, D. (2001) *Biophys. Chem. 89*, 193−199.
23. Marcus, R. A. (1956) *J. Chem. Phys. 24*, 966−978.
24. Voss, E. W. J. (1990) *Comments Mol. Cell. Biophys. 6*, 197−221.
25. Klonis, N., Clayton, A. H. A., Voss, E. W. J., and Sawyer, W. H. (1998) *Photochem. Photobiol. 67*, 500−510.
26. Voss, E. W. J., and Watt, R. M. (1977) *Immunochemistry 14*, 237−246.
27. Watt, R. M., and Voss, E. W. J. (1977) *Immunochemistry 14*, 533−541.
28. Voss, E. W. J., Croney, J. C., and Jamesson, D. M. (2001) *Mol. Immunol. 38*, 35−44.
29. Komazaki, S., Ikegami, I., Forosawa, H., Yasuda, F., and Yoshihara, K. (2001) *J. Phys. Chem. B 105*, 1093−1099.
30. Zinth, W., and Kaiser, W. (1993) *The Photosynthetic Reaction Center*, Vol. 2, Academic Press, New York.
31. Priev, A., Almagor, A., Yedgar, S., and Gavish, B. (1996) *Biochemistry 35*, 2061−2066.
32. Schlichter, J., Friedrich, J., Herenyi, L., and Fidy, J. (2001) *Biophys. J. 80*, 2011−2017.
33. Jortner, J. (1976) *J. Chem. Phys. 64*, 4860−4867.
34. Marcus, R. A., and Sutin, N. (1985) *Biochim. Biophys. Acta 811*, 265−322.
35. Bixon, M., and Jortner, J. (1999) in *Electron Transfer−From Isolated Molecules to Biomolecules* (Jortner, J., and Bixon, M., Eds.) pp 35−202, J. Wiley, New York.
36. Häberle, T., Hirsch, J., Pöllinger, F., Heitele, H., Michel-Beyerle, M. E., Anders, C., Döhling, A., Krieger, C., Rückemann, A., and Staab, H. (1996) *J. Phys. Chem. 100*, 18269−18274.

BI015888Y